12th International Conference on Fracture Mechanics of Concrete and Concrete Structures
FraMCoS-12
B.L.A. Pichler, Ch. Hellmich, P. Preinstorfer (Eds)

https://doi.org/10.21012/FC12.1311
MS07-1:5

# ENHANCING CARBONATION CURING OF WOLLASTONITE-PORTLAND CEMENTITIOUS BLENDS THROUGH 3D-PRINTED VASCULAR NETWORKS

**Y. JU, Y. HUANG, T. LIU AND Y. LI***

* Corresponding author & Presenter: Y. Li
Harbin Institute of Technology, School of Civil and Environmental Engineering
Shenzhen, 518055, China
e-mail: liye0006@e.ntu.edu.sg

**Key words:** Wollastonite, Binary cementitious materials, Carbonation, Vascular networks, Embedded 3D printing

**Abstract:** Wollastonite, a low-lime calcium silicate offers low carbon emissions and forms stable calcium carbonates under carbonation. This study explores the integration of Wollastonite and Portland cement in a blended system designed for carbonation curing. While traditional accelerated carbonation curing improves surface hardness in ordinary Portland cement (OPC), its effectiveness is limited in deeper regions due to restricted $CO_2$ diffusion, which hinders both mechanical enhancement and $CO_2$ sequestration. To address this, a novel approach utilizing embedded 3D-printed vascular networks is introduced, facilitating deeper $CO_2$ penetration and a higher overall carbonation degree. The vascular channels, with diameters of 300, 500, 700, and 900 μm, were evaluated for their impact on the morphology and composition of the channel walls post-carbonation. Additionally, the compressive strength of 500 μm cubic samples oriented radially from the channels was assessed. The results provide valuable insights for optimizing vascular network designs in carbonation-hardened cementitious materials.

## 1 INTRODUCTION

The production of concrete is a significant source of global carbon emissions, releasing over 2.3 billion tons of $CO_2$ annually, which accounts for approximately 5% to 8% of total emissions [1]. Cement as an essential component of concrete, contributes significantly to these emissions, with one ton of clinker production releasing more than 0.8 tons of $CO_2$ [2]. Notably, around 60% of these emissions arise from limestone decomposition during calcination [3]. Given the substantial carbon footprint of the cement industry, mitigating its emissions has become a critical factor in addressing climate change globally. Replacing limestone in the raw material and producing low calcium clinker offers a viable strategy for reducing emissions in the cement industry [4].

Wollastonite, a low-calcium calcium silicate mineral, presents a promising alternative to cement clinker. Its lower calcination temperature (approximately 1100°C) compared to that of ordinary Portland cement (OPC) (1450°C) enables a substantial reduction in carbon emissions during production [5]. Although non-hydraulic, wollastonite can chemically react with $CO_2$, forming calcium carbonate crystals and silica gel [6-8]. Recent studies have explored the potential of activating non-hydraulic calcium silicate minerals with $CO_2$ to develop their mechanical properties. For instance, Gineika et al. [9] synthesized wollastonite from $AlF_3$-rich silica gel and calcium oxide via hydrothermal methods, achieving compressive strengths of

10 to 15 MPa in compacted specimens with varying sand content. Similarly, Ashraf et al. [10] produced compacted specimens from natural wollastonite powder with a water-to-solid ratio of 0.35, achieving compressive strengths of 60 to 80 MPa after 60 to 75 hours of carbonation curing. Given that OPC components such as $C_3S$ and $\beta$-$C_2S$ also react with $CO_2$ [11, 12], combining wollastonite with OPC offers the potential to develop a novel binary cementitious material that reduces the carbon footprint. Carbonation curing is particularly effective in optimizing the mechanical properties of such wollastonite-OPC binary cementitious materials (WPC).

However, carbonation depth and degree in cementitious materials face inherent limitations. The reaction between alkaline substances in cement and $CO_2$ often leads to the formation of passivation layers of silica and carbonate, which impede the transport of metal cations to the reaction surface [13]. While dry and wet carbonation curing techniques attempt to enhance carbonation by increasing reaction temperature, gas pressure, and concentration [14-16], they remain insufficient in significantly improving carbonation depth and degree.

To address this challenge, researchers have drawn inspiration from natural systems such as blood vessels and leaf veins, designing vascular networks to enable self-healing in cementitious materials [17, 18]. For instance, Li et al. [18] developed a 3D vascular network capable of delivering healing agents, achieving over 34% recovery of mechanical properties. Zhang et al. [19] introduced an in-situ embedded printing strategy to construct 3D vascular systems within cementitious materials, enabling autonomous healing behavior. Beyond self-healing, these vascular networks create pathways that facilitate $CO_2$ gas infiltration into deeper zones of cementitious systems, enhancing carbonation reactions and improving mechanical performance in the deeper layers of WPC.

This study investigates the performance of binary cementitious materials composed of wollastonite and OPC, leveraging carbonation curing to enhance mechanical properties. Furthermore, a novel method of embedding 3D-printed vascular networks within WPC paste is proposed and validated to improve carbonation depth and degree in the material's deeper layers.

## 2 MATERIALS AND SAMPLE PREPARATION

### 2.1 Materials

The materials used in this study include wollastonite, Portland cement (P.O 42.5 R, OPC), standard sand, and superplasticizer. The particle size distribution and morphology of the wollastonite particles are presented in Figure 1. The median diameter of the wollastonite particles is 45 μm, indicating a fine particle size suitable for blending with cementitious materials. The aspect ratio of the particles seems high, which may lower the workability. The chemical compositions of OPC and wollastonite are detailed in Table 1.

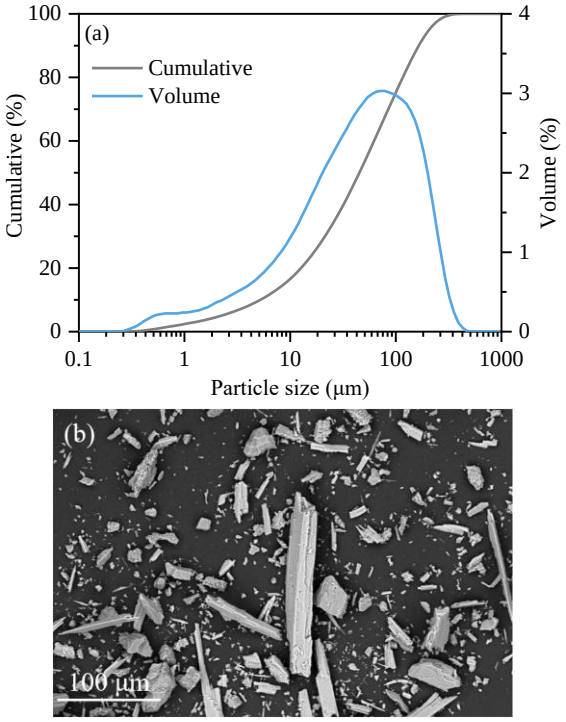


**Figure 1:** (a) Particle size distribution of wollastonite and (b) morphology of wollastonite.

The median diameter of the wollastonite particles is 45 μm, indicating a fine particle size suitable for blending with cementitious

materials. The aspect ratio of the particles seems high, which may lower the workability.

**Table 1:** Composition of OPC and wollastonite.

| Composition (wt. %) | OPC | Wollastonite |
|---|---|---|
| CaO | 61.64 | 44.50 |
| $SiO_2$ | 21.54 | 51.44 |
| $Al_2O_3$ | 5.70 | 0.24 |
| $Fe_2O_3$ | 3.30 | 0.16 |
| MgO | 2.93 | 3.04 |
| $K_2O$ | 1.07 | 0.02 |
| $SO_3$ | 3.24 | 0.68 |

### 2.2 Specimens with embedded 3D-printed vascular networks

To fabricate specimens with embedded vascular networks, a robotic deposition device (TH-206H, Tianhao Technic, China) was employed to print emulgel inks inside the fresh WPC mix, following the method outlined by Zhang et al. [19]. The emulgel inks were extruded through needles of varying diameters (0.3, 0.5, 0.7, and 0.9 mm) at a moving speed of 180 mm/min, as depicted in Figure 2.

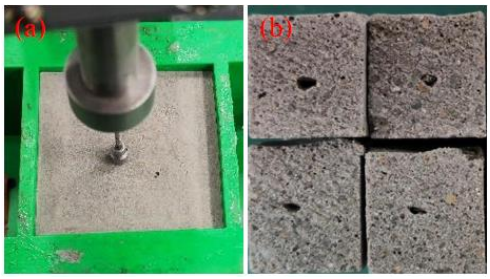


**Figure 2**: Specimens with embedded 3D-printed vascular networks, (a) the procedure of printing emulgel inks, (b) the processed specimens.

WPC specimens were prepared with a water-to-cement ratio of 0.3 and included 0.31 wt.% superplasticizer to ensure proper workability. After fabrication, the specimens were subjected to carbonation curing in a controlled environment chamber at 40°C, 70% relative humidity, and a $CO_2$ concentration of 20%. For comparative analysis, OPC paste specimens were also prepared and cured in water at 20°C. Both sets of specimens were cured for 28 days. To facilitate the analysis of the impact of wollastonite content and curing methods, the specimens were labeled as W/C-30/40/50, where "W" and "C" denote water curing and carbonation curing, respectively, and the numbers (30, 40, 50) indicate the proportion of wollastonite in the mix.

## 3 CHARACTERIZATION METHODS

### 3.1 Mechanical performances

The compressive strength of WPC specimens was tested at both macro and micro scales. At the macro scale, compressive strength tests were performed on 15 mm cubic specimens using a SANS universal testing machine from MTS Ltd. The tests were conducted at a constant displacement rate of 0.3 mm/min, following the protocols outlined in previous studies [20, 21].

At the micro scale, compressive strength tests were carried out on 500 μm cubic specimens using a micro force tester, as described in [22]. The preparation of these specimens involved several precise steps. First, thin WPC plate were ground to the desired thickness and polished sequentially with diamond pastes of decreasing grit sizes (6 μm, 3 μm, and 1 μm), each applied for 15 minutes. After each polishing step, the sheets were cleaned in an ultrasonic bath to remove residues. Once polished, the sheets were cut into 500 μm cubes using a precision micro-dicing saw, ensuring cuts in two perpendicular directions. The resulting specimens are shown in Figure 3.

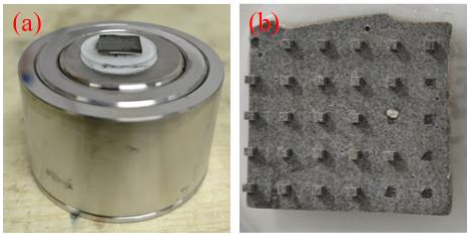


**Figure 3**: 500 μm cubes of WPC specimens, (a) the samples in grinding and polishing, (b) the cut cubes.

### 3.2 Phase assemblage and microstructure characterization

The phase composition and microstructure of WPC specimens were analyzed using X-ray diffraction (XRD), thermogravimetric analysis (TGA), and nuclear magnetic resonance

(NMR) techniques. To prevent ongoing hydration and carbonation during sample preparation, all specimens for these tests were preserved in isopropanol, then milled and sieved through a 75 μm mesh.

XRD analysis was performed using Cu Kα radiation at 40 kV and 40 mA, with scans conducted over a range of 5° to 65° for 20 minutes. Zinc oxide (ZnO) was included at 10% as an internal standard to facilitate quantification of phase composition. For TGA, samples were heated in a nitrogen atmosphere from 30°C to 1000°C at a rate of 10°C/min to assess thermal stability and decomposition profiles. The $^{29}$Si-NMR tests were conducted at a frequency of 119.23 MHz and a spinning rate of 5 kHz, employing 400 scans with π/2 pulses of 11 μs and relaxation delays of 40 seconds.

To quantify the degree of carbonation (DOC) and calcium carbonate ($CaCO_3$) content in the specimens, calculations were performed using weight loss data from TGA results. The content of calcium carbonate was determined using the following equation [23, 24]:

$$m_c(\%) = w_{500-650} \times \frac{M_{CaCO3}}{M_{CO2}} \times 100\% \quad (1)$$

$$DOC(\%) = \frac{m_c \times M_{CaO}}{m_{CaO,WPC} \times M_{CaCO3}} \times 100\% \quad (2)$$

where $m_c$ represents the percentages of $CaCO_3$. $w_{500\text{-}800}$ is the relative weight loss between 500 to 800°C. $M_{CaCO_3}$, $M_{CO_2}$, and $M_{CaO}$ are the molar masses of $CaCO_3$, $CO_2$, and CaO, respectively. $m_{CaO,WPC}$ represents the calcium oxide content of the WPC samples shown in **Error! Reference source not found.**.

The microstructure and porosity of the WPC specimens were further examined using mercury intrusion porosimetry (MIP). Samples were extracted from the central regions of the specimens, and pore sizes ranging from 6 nm to 360 μm were analyzed under pressures varying from 0 to 227 MPa. The carbon distribution in specimens with embedded 3D-printed vascular networks was analyzed using a Phenom Prox G6 scanning electron microscope (SEM) equipped with energy-dispersive X-ray spectroscopy (EDS).

## 4 RESULTS AND DISCUSSION

### 4.1 Properties of WPC specimens

The compressive strengths of WPC specimens with varying wollastonite content and curing methods are shown in Figure 4. Specimens cured under carbonation exhibit significantly higher compressive strengths, reaching a maximum of 94.9 MPa, compared to their water-cured counterparts. Across all curing methods, the compressive strength decreases as the wollastonite content increases. This trend highlights the inverse relationship between wollastonite content and mechanical performance due to its predominantly inert nature.

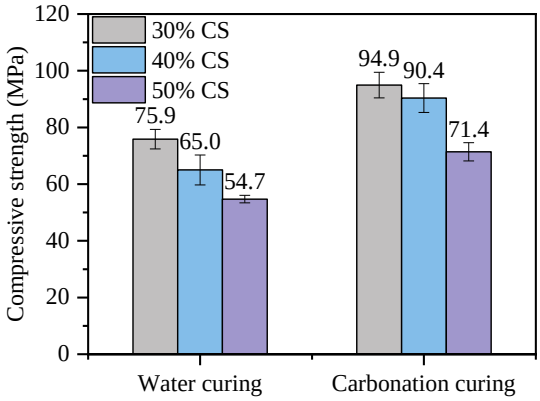


**Figure 4**: Compressive strength of WPC specimens.

The pore structure and porosity of the WPC specimens were shown in Figure 5. Water-cured samples exhibit increased pore sizes and porosity with higher wollastonite content, reflected by the rightward shift of the pore size distribution peak. Wollastonite, with a median particle size of 45 μm, acts as a filler in these samples [25]. When the wollastonite content reaches 50%, the W-50 sample shows two distinct pore peaks, with porosity increasing to 28.5%.

In contrast, carbonated specimens show significantly reduced porosities compared to water-cured specimens. This reduction occurs because carbonation reactions between $CO_2$ and OPC components ($C_3S$ and β-$C_2S$) form

calcium carbonate ($CaCO_3$) polymorphs, while wollastonite reacts to produce $CaCO_3$ and silica gel. These reactions fill the pores, enhance densification, and contribute to improved mechanical strength. However, the carbonated samples exhibit larger peak pore sizes than water-cured samples, possibly due to the localized precipitation of $CaCO_3$ near calcium silicate phases or hydration products, with limited production between mineral particles [21].

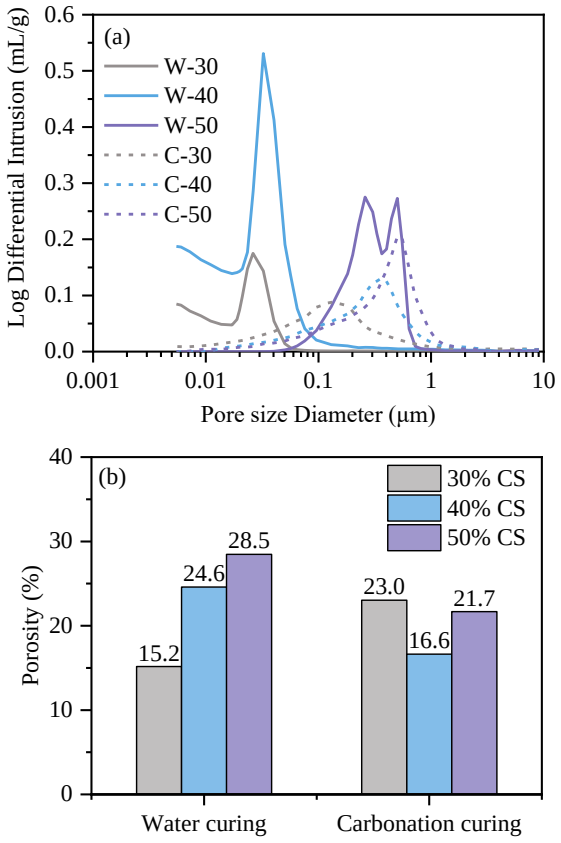


**Figure 5:** MIP results of WPC specimens (a) pore distribution curves and (b) porosity.

The phase composition and microstructural characteristics of WPC specimens are presented in Figure 6. The carbonation products differ notably from hydration products. As wollastonite content increases, the amount of unreacted wollastonite (CS) in water-cured samples rises, as seen in Figure 6 (b), while amorphous content decreases. The amorphous phase, identified in Figure 6 (f) by $Q^1$ and $Q_b^2$ peaks, primarily consists of C-S-H gel [26]. The hydration reactions of $C_3S$ and β-$C_2S$ generate calcium hydroxide (CH) and C-S-H gel, as illustrated by Figure 6 (c). The increasing presence of unreacted wollastonite in water-cured samples acts as an inert filler, reducing the production of hydration products and, consequently, compressive strength.

In carbonated samples, wollastonite content decreases by 11.4%, 13.9%, and 18.2% for C-30, C-40, and C-50, respectively, while $CaCO_3$ polymorph production increases by 27.8%, 25.6%, and 23.1%, respectively. Figure 6 (e) and Figure 6 (f) show that the carbonated samples contain $C_3S$ and β-$C_2S$ ($Q^0$), unreacted wollastonite ($Q^2$), C-S-H gel ($Q^1$ and $Q_b^2$), calcium-modified silica gel ($Q^3$(Ca) and $Q^3$(OH)), and silica gel ($Q^4$) [26-28]. The amorphous phase in carbonated specimens includes C-S-H gel formed through hydration and silica-based gels produced through carbonation. Silica gel, formed directly from the reaction of wollastonite with $CO_2$, exhibits a high degree of polymerization. As wollastonite content increases, the relative intensity of $Q^4$ in carbonated samples also rises.

Different curing methods influence the transformation of hydration products (e.g., calcium hydroxide) to carbonation products (e.g., calcium carbonate polymorphs). Water-cured samples are dominated by C-S-H gel, while carbonated specimens exhibit a combination of C-S-H gel, calcium-modified silica gel, and silica gel. The carbonation products, such as calcite, calcium-modified silica gel, and silica gel, possess higher elastic moduli compared to hydration products like CH and C-S-H gel [10, 29]. This transformation contributes to the enhanced mechanical performance of carbonated specimens. Consequently, wollastonite can effectively replace a portion of OPC in WPC mixtures, enabling the preparation of high-performance binary cementitious materials under carbonation curing.

Despite these improvements, carbonated specimens still contain unreacted wollastonite. Figure 6 (d) shows that the degree of carbonation (DOC) decreases with increasing wollastonite content, indicating that carbonation reactions in WPC specimens remain incomplete. Full carbonation

throughout the specimens is not achieved, limiting the mechanical contributions of calcium carbonate crystals. To address this limitation, further research should focus on enhancing carbonation depth and degree to maximize the formation of carbonation products and improve mechanical properties.

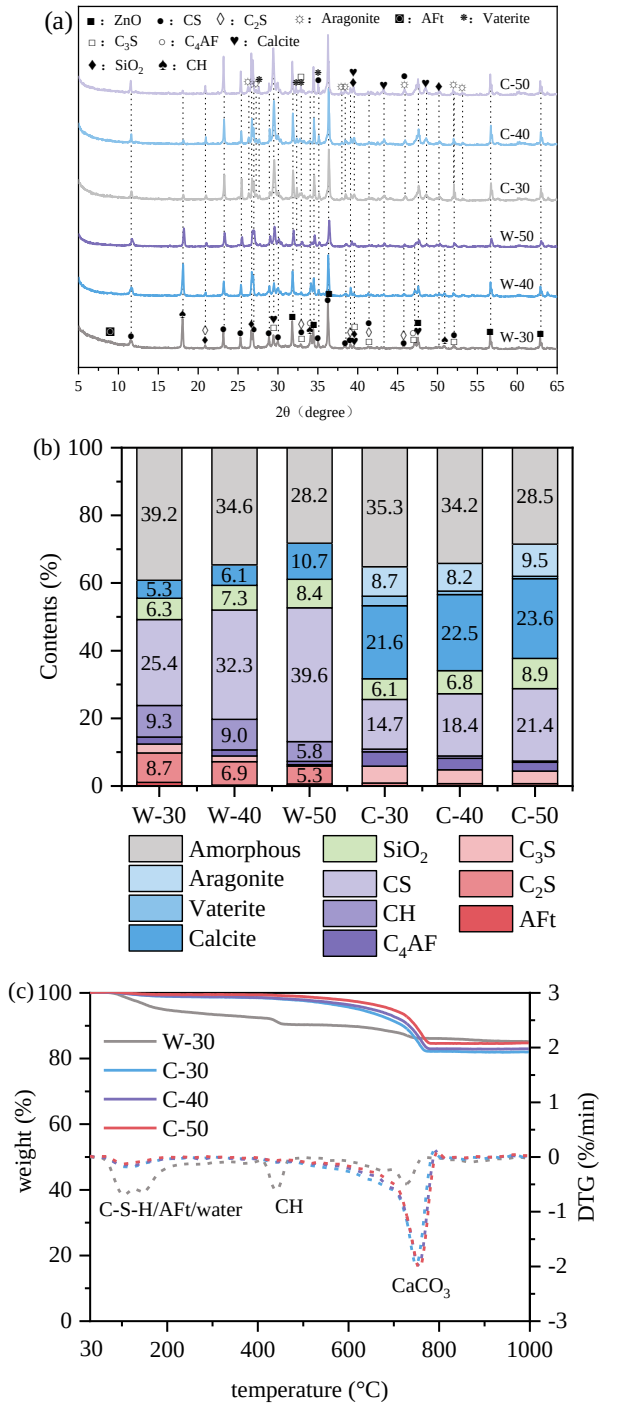


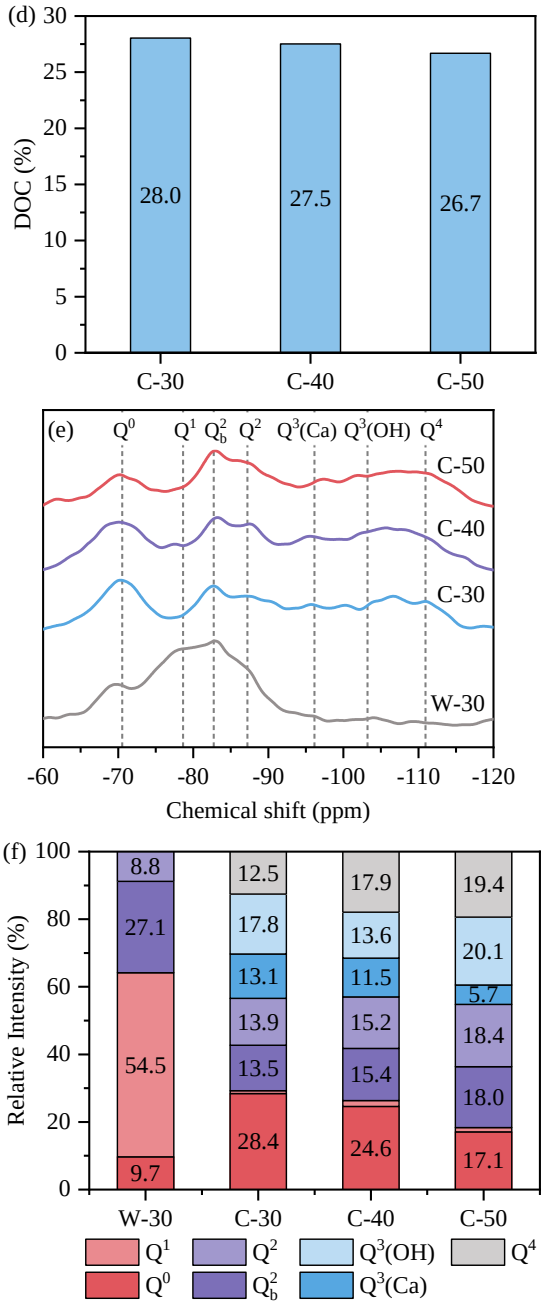


**Figure 6:** (a) X-ray diffraction pattern, (b) phase assemblage based on the XRD pattern, (c) TG curves, (d) degree of carbonation, (e) $^{29}$Si-NMR spectrum, and (f) relative peak area based on the $^{29}$Si-NMR spectrum results of WPC specimens.

## 4.2 Optimized WPC specimens with 3D-printed vascular networks

The effectiveness of embedded 3D-printed vascular networks in improving carbonation depth and mechanical properties of WPC specimens was investigated by varying the inner channel diameters. Figure 7 illustrates the carbonation depths for WPC specimens

embedded with a single-channel vascular system of different diameters after 7 days of carbonation. Embedding a single-channel vascular system significantly increased the fully carbonated region in the specimens. The smallest carbonation depth, approximately 2.1 mm, was observed for the 0.3 mm channel, while specimens with 0.5 mm, 0.7 mm, and 0.9 mm channels exhibited carbonation depths of 3.8 mm, 3.4 mm, and 3.9 mm, respectively. The limited enhancement in carbonation depth for the 0.3 mm channel is attributed to its restricted ability to expand the contact region between $CO_2$ gas and the specimen.

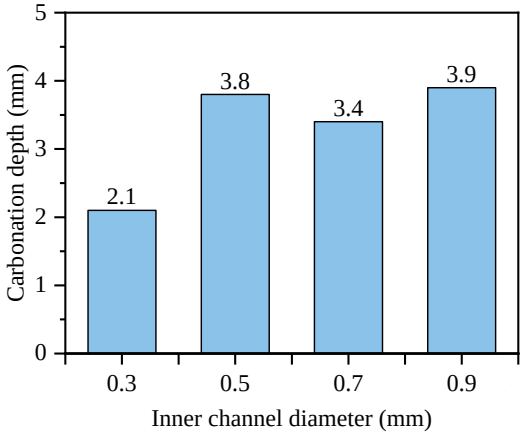


**Figure 7:** Carbonation depths of WPC specimens embedded 3D-printed vascular networks.

The compressive strength of local cement paste measured by the micro scale 500 μm cubes and carbon concentration varied with the distance from the embedded channels, as shown in Figure 8. For specimens with a 0.3 mm channel, the highest compressive strength of 131.1 MPa was recorded at a distance of 2.2 mm from the channel, where carbon concentration exceeded 19%, indicating a substantial production of calcium carbonate. Between 2.2 mm and 4 mm, compressive strength rapidly declined to 52.9 MPa at 4 mm, with a corresponding decrease in carbon concentration to 15.6%. Beyond 4 mm, compressive strength stabilized at approximately 50 MPa, with carbon concentrations ranging from 16% to 18%. This behavior reflects a common carbonation phenomenon in WPC, where proximity to the channel promotes the formation of a dense region of carbonation products that enhances mechanical strength [23]. At 1 mm from the channel, despite a high carbon concentration of 21%, compressive strength was only 79.5 MPa, approximately 60.6% of the maximum value, likely due to pores introduced by the vascular networks.

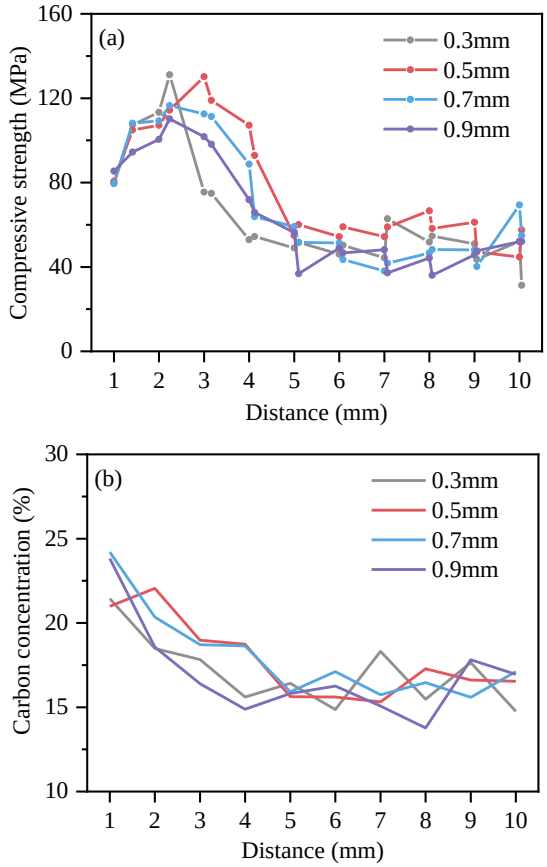


**Figure 8:** (a)The compressive strength and (b) carbon concentration at different distances from the vascular networks.

For specimens with a 0.5 mm channel, the maximum compressive strength of the 500 μm cubes was 130.2 MPa observed at 3 mm from the channel. Compressive strength decreased from 100 MPa to 54.8 MPa between 2 mm and 4 mm, eventually stabilizing at 55 MPa for cubes located beyond 5 mm from the channel. Specimens with channel diameters of 0.7 mm and 0.9 mm exhibited similar trends, with peak compressive strengths of 116.5 MPa and 110.2 MPa observed at 2.2 mm from the channel. Beyond this distance, compressive strength decreased, eventually stabilizing at approximately 50 MPa.

These results demonstrate that embedded

3D-printed vascular networks create a hardened region around the internal channels, filled with carbonation products, which enhances carbonation degree and compressive strength at the micrometer scale. This localized improvement in mechanical properties may also contribute to higher compressive strengths at the macro scale. Future studies should explore the impact of vascular networks on macro-scale mechanical performance, considering factors such as the spacing and spatial arrangement of multiple channels to optimize carbonation and mechanical capacity.

## 5 CONCLUSIONS

This study investigated the performance of wollastonite-Portland cement (WPC) binary cementitious systems with embedded 3D-printed vascular networks, aiming to optimize the use of natural wollastonite and enhance the mechanical properties of carbonation-hardened materials. By developing a novel method to quantitatively assess the compressive strength of 500 μm cubes at the micrometer scale, alongside complementary analyses using XRD, $^{29}$Si-NMR, TGA, and MIP, the study revealed key findings. Carbonated WPC specimens achieved excellent macroscopic mechanical properties, with compressive strength reaching 94.9 MPa, significantly surpassing water-cured counterparts. Although increasing wollastonite content reduced compressive strength due to its inert filler nature, carbonation curing activated wollastonite, forming calcium carbonate and silica gel that enhanced mechanical performance. Additionally, 3D-printed vascular networks improved the degree of carbonation and compressive strength at the micrometer scale by facilitating $CO_2$ penetration, creating hardened regions enriched with calcium carbonate along channel walls. These findings underscore the potential of WPC systems with embedded vascular networks as a sustainable approach for optimizing carbonation curing and enhancing mechanical performance.

## ACKNOWLEDGMENTS

This work was supported by the National Science Fund for Distinguished Young Scholars (No. 52025081), the National Natural Science Foundation of China (U23A20658, 52378229), and the Science and Technology Planning Project of Guangdong Province (2023A0505050098).

## REFERENCES

[1] Cavalett, O., Watanabe, M.D.B., Voldsund, M., et al., 2024. Paving the way for Sustainable Decarbonization of the European Cement Industry. *Nat. Sustain.* **7**:568-80.

[2] Maddalena, R., Roberts, J.J. and Hamilton, A., 2018. Can Portland Cement be Replaced by Low-carbon Alternative Materials? A Study on the Thermal Properties and Carbon Emissions of Innovative Cements. *J. Clean. Prod.* **186**:933-42.

[3] Farfan, J., Fasihi, M. and Breyer, C., 2019. Trends in the Global Cement Industry and Opportunities for Long-term Sustainable CCU Potential for Power-to-X. *J. Clean. Prod.* **217**:821-35.

[4] Habert, G., Miller, S.A., John, V.M., et al., 2020. Environmental Impacts and Decarbonization Strategies in the Cement and Concrete Industries. *Nat. Rev. Earth Environ.* **1**:559-73.

[5] Kotsis, I. and Balogh, A., 1989. Synthesis of Wollastonite. *Ceramics International*. **15**:79-85.

[6] Huijgen, W.J.J., Witkamp, G.-J. and Comans, R.N.J., 2006. Mechanisms of Aqueous Wollastonite Carbonation as a Possible $CO_2$ Sequestration Process. *Chem. Eng. Sci.* **61**:4242-51.

[7] Ashraf, W. and Olek, J., 2016. Carbonation Behavior of Hydraulic and Non-hydraulic Calcium Silicates: Potential of Utilizing Low-lime Calcium

Silicates in Cement-based Materials. *J. Mater. Sci.* **51**:6173-91.

[8] Daval, D., Martinez, I., Corvisier, J., et al., 2009. Carbonation of Ca-bearing Silicates, the Case of Wollastonite: Experimental Investigations and Kinetic Modeling. *Chem. Geol.* **265**:63-78.

[9] Gineika, A., Siauciunas, R. and Baltakys, K., 2019. Synthesis of Wollastonite from $AlF_3$-rich Silica Gel and its Hardening in the $CO_2$ Atmosphere. *Sci Rep*. **9**:18063-73.

[10] Ashraf, W., Olek, J. and Tian, N., 2016. Multiscale Characterization of Carbonated Wollastonite Paste and Application of Homogenization Schemes to Predict its Effective Elastic Modulus. *Cem. Concr. Compos.* **72**:284-98.

[11] Zhao, S.X., Liu, Z.C., Wang, F.Z., et al., 2021. Effect of Extended Carbonation Curing on the Properties of γ-$C_2S$ Compacts and Its Implications on the Multi-step Reaction Mechanism. *ACS Sustain. Chem. Eng.* **9**:6673-84.

[12] Wang, D., Fang, Y.F., Zhang, Y.Y., et al., 2019. Changes in Mineral Composition, Growth of Calcite Crystal, and Promotion of Physico-chemical Properties Induced by Carbonation of β-$C_2S$. *J. CO2 Util.* **34**:149-62.

[13] Walker, I., Bell, R. and Rippy, K., 2024. Mineralization of Alkaline Waste for CCUS. *npj Materials Sustainability*. **2**:28-45.

[14] Chang, R.G., Kim, S.M., Lee, S.I., et al., 2017. Calcium Carbonate Precipitation for $CO_2$ Storage and Utilization: A Review of the Carbonate Crystallization and Polymorphism. *Front. Energy Res.* **5**:

[15] Fernandez Bertos, M., Simons, S.J., Hills, C.D., et al., 2004. A Review of Accelerated Carbonation Technology in the Treatment of Cement-based Materials and Sequestration of $CO_2$. *J Hazard Mater*. **112**:193-205.

[16] Mao, Y.G., He, P.P., Drissi, S., et al., 2023. Effect of Conditions on Wet Carbonation Products of Recycled Cement Paste Powder. *Cem. Concr. Compos.* **144**:105307-28.

[17] Van Tittelboom, K. and De Belie, N., 2013. Self-Healing in Cementitious Materials-A Review. *Materials*. **6**:2182-217.

[18] Li, Z.J., Souza, L.R.d., Litina, C., et al., 2020. A Novel Biomimetic Design of a 3D Vascular Structure for Self-healing in Cementitious Materials using Murray's Law. *Mater. Des.* **190**:108572-86.

[19] Zhang, Y.Y., Pan, P., Li, W.Q., et al., 2022. Freeform Embedded Printing of Vasculature in Cementitious Materials for Healing-agent Transport. *Addit. Manuf.* **59**:103140-49.

[20] Wang, D., Xiong, C., Li, W.Z., et al., 2020. Growth of Calcium Carbonate Induced by Accelerated Carbonation of Tricalcium Silicate. *ACS Sustain. Chem. Eng.* **8**:14718-31.

[21] Mu, Y.D., Liu, Z.C. and Wang, F.Z., 2019. Comparative Study on the Carbonation-activated Calcium Silicates as Sustainable Binders: Reactivity, Mechanical Performance, and Microstructure. *ACS Sustain. Chem. Eng.* **7**:7058-70.

[22] Zhang, H.Z., Xu, Y.D., Gan, Y.D., et al., 2019. Combined Experimental and Numerical Study of Uniaxial Compression Failure of Hardened Cement Paste at Micrometre Length Scale. *Cem. Concr. Res.* **126**:105925-40.

[23] Zhan, B.J., Xuan, D.X., Poon, C.S., et al., 2021. Multi-scale Investigation on Mechanical Behavior and Microstructural

Alteration of C-S-H in Carbonated Alite Paste. *Cem. Concr. Res.* **144**:106448-80.

[24] Andrade, C., 2020. Evaluation of the Degree of Carbonation of Concretes in Three Environments. *Constr. Build. Mater.* **230**:

[25] Juenger, M.C.G. and Siddique, R., 2015. Recent Advances in Understanding the Role of Supplementary Cementitious Materials in Concrete. *Cem. Concr. Res.* **78**:71-80.

[26] Ashraf, W. and Olek, J., 2018. Elucidating the Accelerated Carbonation Products of Calcium Silicates Using Multi-technique Approach. *J. CO2 Util.* **23**:61-74.

[27] Liu, W., Li, Y.-Q., Tang, L.-P., et al., 2019. XRD and $^{29}$Si MAS NMR Study on Carbonated Cement Paste under Accelerated Carbonation using Different Concentration of $CO_2$. *Mater. Today Commun.* **19**:464-70.

[28] Sevelsted, T.F. and Skibsted, J., 2015. Carbonation of C-S-H and C-A-S-H Samples Studied by $^{13}$C, $^{27}$Al and $^{29}$Si MAS NMR Spectroscopy. *Cem. Concr. Res.* **71**:56-65.

[29] Chen, J.J., Sorelli, L., Vandamme, M., et al., 2010. A Coupled Nanoindentation/SEM-EDS Study on Low Water/Cement Ratio Portland Cement Paste: Evidence for C-S-H/$Ca(OH)_2$ Nanocomposites. *J. Am. Ceram. Soc.* **93**:1484-93.